Solvation Behavior of Short-Chain Polystyrene Sulfonate in Aqueous Electrolyte Solutions: A Molecular Dynamics Study

Ariel A. Chialvo* and J. Michael Simonson

Chemical Sciences Division, Aqueous Chemistry and Geochemistry Group, Oak Ridge National Laboratory, Oak Ridge, Tennessee 37831-6110

We analyze the solvation behavior of short-chain polystyrene sulfonate (PSS) in aqueous electrolyte solutions by isothernal–isochoric molecular dynamics simulation to determine the solvation effects on the structure and conformation of the polyelectrolyte as a function of the aqueous environment. To that end, we study these aqueous systems including the explicit atomistic description of water, the PSS chain, and their interactions with all species in solution. In addition, we investigate the effect of the degree of sulfonation and its distribution along the PSS chain on the resulting conformation as well as solvation structure. Moreover, we assess the impact of added salts on the net charge of the PSS backbone, placing emphasis on the valence of the counterion and the extent of the ion-pair formation between the sulfonate group and the counterions. Finally, we present evidence for the so-called *like-charge attraction* between sulfonate groups through the formation of counterion-mediated interchain sulfonate–sulfonate and water-mediated intrachain sulfonate–sulfonate bridges, as well as between unlike counterion–counterion interactions.

1. Introduction

Polyion–counterion interactions play an essential role in determining the stability and solubility of polyelectrolytes in aqueous solutions [1]. These interactions are particularly strong for multivalent counterions, common in biological systems,[2–5] where the negatively charged biopolymer interacts with divalent and trivalent metal ions. The nature of the counterion [6] in these systems, including its electrostatic charge [7] and the short-range interaction [8] with the binding site of the polyelectrolyte, appears to be as important as the location of the binding site in the backbone.[9] Consequently, the binding between the polyelectrolyte charged sites and the counterions (counterion condensation) can exhibit a marked ion selectivity, resulting from a delicate balance between short-range (solvation) interactions characterizing the local environment and long-range (though partially screened by the presence of ions) electrostatic interactions,[10] that leads to ion-pair association (i.e., between ions of the added salt and the original counterions) and counterion condensation (i.e., between the charged backbones and any counterion). The local environment around the charge species depends strongly on the solvent's properties, the ionic strength, as well as the state conditions, and therefore, it becomes significantly different from that characterized by a solvent as a continuum dielectric.[11]

All of these observations indicate that the chain conformation and the structure of the solution might depend on several factors, including (a) the structure of the chain backbone and the distribution of charges of the polyelectrolyte, (b) the charge and concentration of the counterions as well as the presence of salts, and (c) the strength of the interactions between the solvent and both the polyelectrolyte and the counterions (solvation effects). Thus, because the occurrence of ion-pair formation and counterion condensation depends on the actual properties of the solvent in the ion's local environment, it is crucial to address explicitly the participation of the solvent,[12] i.e., not as a dielectric continuum but as an atomistically discrete molecular entity.

This situation points to the need for a more detailed understanding of the polyion–counterion behavior in aqueous and aqueous–electrolyte solutions. For example, the understanding of the mechanism underlying the ion selectivity (and eventual counterion condensation) of highly charged polyelectrolytes in the presence of monovalent counterions is central to the quantitative interpretation of a variety of experimental measurements of the physicochemical properties of polyelectrolytes in solution. Most studies invoke the concept of an *effective charge* for the polyelectrolyte chain in solution,[13] resulting from the partial charge screening by ion pairing between the charged sites in the chain (i.e., the intrinsic or bare charge) and the counterions in solution, to approximate the connections between chain conformation and counterion distribution and eventual condensation.[6] Unfortunately, this *effective*, as opposed to the *intrinsic*, charge is not a thermophysical property of the system, and consequently, it cannot be measured directly.[14] While there are a few available techniques to evaluate this effective charge, including osmometry,[15] electrophoresis NMR,[16] dielectric spectroscopy,[17] and electric conductivity,[18] the relationship between the experimental and the derived effective charge is model dependent,[19] and usually the effective charge becomes an adjustable parameter.[20,21]

The purpose of this work is to address specific aspects of structural and conformational behavior of short polyelectrolyte chains in the presence (or absence) of added salt in aqueous solutions. We focused our attention on short polystyrene sulfonate chains composed of 8-mers, modeled according to a united-atom description for the CH, CH_2, and CH_3 groups in the alkyl branches and the aromatic rings, as well as for the sulfonate groups.

This simulation study complements both theoretical and experimental investigations of aqueous polyelectrolytes carried

* Corresponding author. E-mail: chialvoaa@ornl.gov. FAX: 865-574-4961.

out in our laboratory[22,23] and differs from other current studies in a few fundamental aspects. Limiting the polyelectrolyte model to relatively short chains in the united-atom approximation makes it computationally tractable to include an explicit and realistic description of water, its interaction with ionomers, and with other species in solution,[11] as opposed to the traditional primitive dielectric continuum picture of the solvent and the consequent dielectrically attenuated Coulombic interactions among all charged species.[24,25] Thus, this approach offers the opportunity to assess specific solvation factors affecting the (configurational and conformational) structure and dynamics of dissolved polyelectrolytes and chain stability, including ion-pair formation. We apply realistic representations of the salts in solution, on the basis of the accurate parametrization of aqueous metal ions,[26,27] in contrast to the generalized use of equal-sized charged spheres in primitive model approaches.[28,29] The information obtained on the strength of all pairwise interactions and their effects on the equilibrium properties of the system suggests possible directions in the design and synthesis of new ionomers for further experimental studies. We investigate the effect of the degree of sulfonation, and its distribution along the chain backbone, on the resulting conformational and solvation structure, with an explicit account for the occurrence of ion-pair association and counterion condensation. Monitoring the configurational and conformational equilibrium of the system through the determination of the configurational temperature simultaneously with the conventional kinetic temperature provides a check for the proper equilibration of slow relaxation processes.

In Section 2, we describe the intermolecular potential models and the molecular simulation methodology, including details on the determination of configurational and conformational properties. In Section 3, we present and discuss the microstructural and conformational behavior of the system, placing emphasis on the geometrical arrangements of condensed counterions as well as the solvation behavior of all ions in solution. Finally, we describe some central features of the solvation behavior of these short PSS chains and discuss the outlook.

2. Potential Models and Simulation Methodology

We have performed isothermal−isochoric molecular dynamics simulations of the aqueous polyelectrolyte solutions consisting of 4000 water molecules, 10 polystyrene sulfonate (PSS) octamers, and the corresponding counterions. For the $s\%$ sulfonate case, with no added salt, $0.80 \times s$ lithium ions were used as counterions (e.g., for 100% sulfonate, 80 monovalent counterions keep the system's electroneutrality). Otherwise, when salt was added to study the effect of polyvalent cations on solvation behavior, chloride ions were used to keep the systems' electroneutrality (see Table 1). Water was described by the SPC/E model,[30] Li^+ and Ba^{2+} according to Aqvist,[26] Cl^- according to Smith and Dang,[31] and van Veggel's parametrization for La^{3+},[27] respectively.

For the octamer backbone, we used the Lyulin and Michels'[32] modification of Mondello et al.'s united atom polystyrene PS model[33] to which we attached the united-atom description of the sulfonate group by Faeder and Ladanyi.[34] In addition to the 100% sulfonate, we also analyzed two possible 50% sulfonate group distributions, i.e., a "block" configuration where all sulfonate groups are located in contiguous phenyl groups, and the "alternated" configuration where these groups are located on every other phenyl group in the chain.

TABLE 1: State Conditions and Composition of Aqueous Systems

no. PSS	% SO_3^-	no. H_2O	no. Li^+	no. Ba^{2+}	no. La^{3+}	no. Cl^-	ρ (g/cc)
10	100	4000	80	0	0	0	1.06
10	50-block	4000	40	0	0	0	1.04
10	50-altern	4000	40	0	0	0	1.04
10	100	4000	80	20	0	40	1.09
10	100	4000	80	0	20	60	1.09
10	100	4000	80	40	0	80	1.09
10	100	4000	80	0	40	120	1.09
10	100	$\epsilon_V = 78^a$	80	0	0	0	0.186
10	50-block	$\epsilon_V = 78$	40	0	0	0	0.147
10	50-altern	$\epsilon_V = 78$	40	0	0	0	0.147
0	$N = 80^b$	4000	80	20	0	40	1.09
0	$N = 80$	4000	80	0	20	60	1.09

^{a} Dielectric continuum. ^{b} Number of sulfonate spheres.

NVT-MD simulations were performed according to the Martyna−Tuckermann−Klein (MTK) explicit reversible integrator,[35] following the scheme presented by Cheng and Merz[36] except for the substitution of the original dual SHAKE[37]-RATTLE[38] routine calls by a single SHAKE routine call through the use of the scheme suggested by Palmer.[39] This substitution makes possible a more efficient scheme for the simultaneous fulfillment of all constraints and their time derivatives, an approach that was successfully applied in our earlier simulation studies of ion-pair formation.[40,41]

All simulations were started from fcc−water configurations, with the "flattened" octamers sandwiched between water layers and the ions randomly distributed in the simulation box. These structures were first melted and equilibrated for at least 200 ps prior to the accumulation of the corresponding quantities for the calculation of their averages, over 4 ns of phase-space trajectory, using a time-step size of 2.0 fs. These quantities comprised the conformational properties of the octamers, such as the root-mean-square radius of gyration (see eq 4) and the root-mean-square end-to-end distance (see eq 5), as well as the configurational properties of the solutions, including the internal energy and the site−site radial distribution functions for water−water, ion−water, ion−chain, chain−water, and chain−chain interactions. Moreover, to verify the proper conformational and configurational equilibration, we have monitored the configurational temperatures[42] (see Appendix A for details) in addition to the usual kinetic temperature.

The total interaction potential for the aqueous PSS system was written in terms of inter- and intramolecular interactions, $U = U_{inter} + U_{intra}$, such that,

$$U_{intra} = \sum_i k_\theta^{aliph}(\theta_i^{aliph} - \theta_o^{aliph})^2 +$$
$$\sum_i k_\varphi^{aliph}(1 - \cos3\varphi_i^{aliph}) + \sum_i k_\chi\cos^2(\chi_i - \chi_o) + \sum_i k_\psi\psi_i^2 +$$
$$\sum_i k_\theta^{arom}(\theta_i^{arom} - \theta_o^{arom})^2 + \sum_i k_\varphi^{arom}(1 - \cos2\varphi_i^{arom}) +$$
$$\sum_i k_\theta^S(\theta_i^S - \theta_o^S)^2 + U_{improper} \quad (1)$$

where the k_θ^{group} terms (with group = aliph, arom, and S) describe the bending potentials for the aliphatic backbone, the phenyl rings, and the sulfonate groups, k_φ^{group} terms describe the torsional potentials for the aliphatic backbone and the phenyl rings, the k_χ term accounts for the torsion of the phenyl ring around the aliphatic−aromatic bond, and the k_ψ term accounts for the phenyl out-of-plane bending potential. In addition, the improper torsional potential, $U_{improper}$, used to prevent the

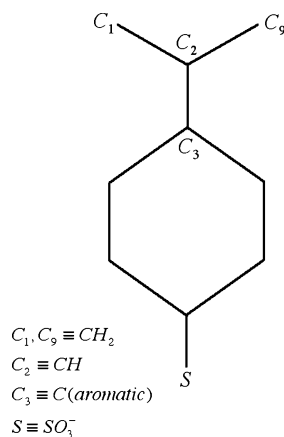Polystyrene Sulfonate in Aqueous Electrolyte Solutions

J. Phys. Chem. B, Vol. 109, No. 48, 2005 **23033**

$C_1, C_9 \equiv CH_2$

$C_2 \equiv CH$

$C_3 \equiv C(aromatic)$

$S \equiv SO_3^-$

Figure 1. Schematic representation of the monomer of the polystyrene sulfonate.

collapsing of the four united atoms, C_1, C_2, C_3, and C_9, onto a plane (see Figure 1), is given by[43]

$$U_{\text{improper}} = 25k_\theta^{\text{aliph}}[(\cos\theta_{129} - \cos\theta_o^{\text{imp}}) + (\cos\theta_{123} - \cos\theta_o^{\text{imp}}) + (\cos\theta_{329} - \cos\theta_o^{\text{imp}})]^6 \quad (2)$$

where $\theta_{\alpha\beta\gamma}$ denotes the bending angle formed by the sites C_α, C_β, and C_γ (see Figure 1).

Finally, the intermolecular water−water, ion−water, chain−water, chain−chain, ion−chain, and ion−ion interactions, U_{inter}, are described by the corresponding Lennard−Jones and Coulombic interactions, i.e.,

$$U_{\text{inter}}(r < r_c) = \sum_{|i-j|\geq 3} [4\epsilon_{ij}\{(\sigma_{ij}/r_{ij})^{12} - (\sigma_{ij}/r_{ij})^6\} + (q_iq_j/r_{ij})] \quad (3)$$

where the unlike pair interaction parameters σ_{ij} and ϵ_{ij} are determined by the Lorentz−Berthelot combining rules. All inter- and intramolecular potential parameters involved in eqs 1−3 are given in Tables B1−B4 of Appendix B. Bonded and nonbonded interactions were truncated at $r_c = 4.5\sigma_{\text{SPC/E}}$, and the long-range Coulombic interactions were accounted for by using an Ewald summation, whose convergence parameters were chosen to obtain an error smaller than $5.10^{-5}\epsilon_{\text{SPC/E}}$ for both the real and reciprocal spaces, i.e., $\alpha \approx 0.18$ Å^{-1} and max $(l, m, n) \approx 9$.[44]

To characterize the structure of the aqueous solution and interpret the solvation behavior of the oligomers in solution, we determined the radial distribution functions for pairs of selected and/or relevant sites, including the three sites of the water model, the sulfonate group and the center of mass of the aromatic rings, and the ions in solutions. Moreover, we studied the sulfonate−counterion pair formation (i.e., counterion condensation), according to the Poirier and DeLap formalism,[45] to take advantage of the ion-pair radial distribution functions in the determination of the degree of association (see Appendix C for details), and implemented an alternative simulation scheme to avoid the problems associated with those cases where the above formalism cannot provide an explicit expression in terms of the conventional ion−counterion radial distribution functions.

To interpret the conformational changes of the oligomer chains, we determined the root-mean-square radius of gyration R_G and the root-mean-squared end-to-end distance R_{ee}, i.e.,

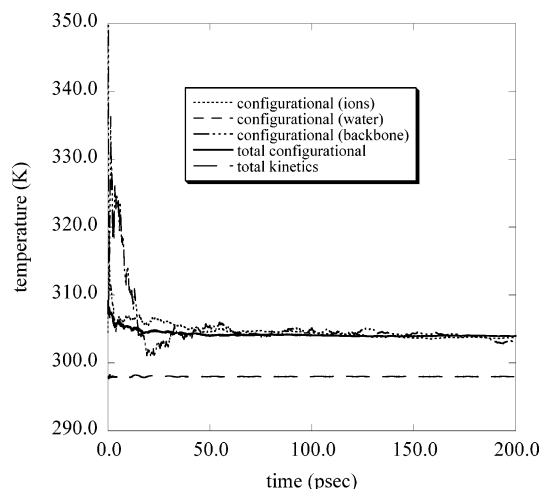$$R_G = \langle\sum_i m_i(r_i - r_{\text{com}})^2 / \sum_i m_i\rangle^{0.5} \quad (4)$$

Figure 2. Time evolution of the configurational temperature in comparison to the kinetic temperature.

where $(r_i - r_{\text{com}})$ is the position of site i relative to the oligomer's center of mass r_{com}, m_i is the corresponding site mass, and $\langle\cdots\rangle$ denotes a simulation average. Likewise,

$$R_{ee} = \langle(r_1 - r_N)^2\rangle^{0.5} \quad (5)$$

where $(r_1 - r_N)$ is the relative position of one end of the chain with respect to the other end.

In addition to the aqueous PSS solutions with explicit description of the solvent, we analyzed the behavior of some aqueous systems, where the PSS chains are replaced by the corresponding sulfonate ions (S), to determine the effect of the PSS backbone on the solvation behavior of the species in solution. Finally, we studied a few systems without added salts, where the solvent was implicitly described by a continuum dielectric counterpart (primitive model), to assess the solvation effects on the structural and conformational properties of the system, as indicated in Table 1. Those simulations were started with the final configurations of the corresponding systems involving the explicit solvent, replacing all electrostatic interactions by the dielectric attenuated ones, and zeroing all explicit interactions involving the solvent.

3. Microstructural and Conformational Results

In what follows, we present the predicted microstructural behavior of the systems and discuss its implications for some relevant pair interactions. All these properties were accumulated after the system reached the proper kinetic and configurational equilibration, as indicated by the corresponding kinetic and configurational temperatures in Figure 2 for a representative system. This figure indicates that not only the system as a whole, but also each of the three subsystems (i.e., the water, the ions, and the backbones) converge to the same configurational temperature whose value, as expected (see Appendix A), deviates by ∼1.6% from the corresponding kinetic counterpart.

3.1. Water−Water Interactions. In Figure 3a−c, we display a representative set of site−site radial distribution functions for water in the aqueous polyelectrolyte (PSS) solutions in comparison with those from a "backbone-free" electrolyte (S) solution counterparts. While there are clearly some small differences among the corresponding radial distribution functions, the presence of the backbone and its degree of sulfonation appear to have a weak impact on the water structure, at least for these low backbone and ionic concentrations. Note, however, the subtle but relevant slowly decaying tails in the distribution
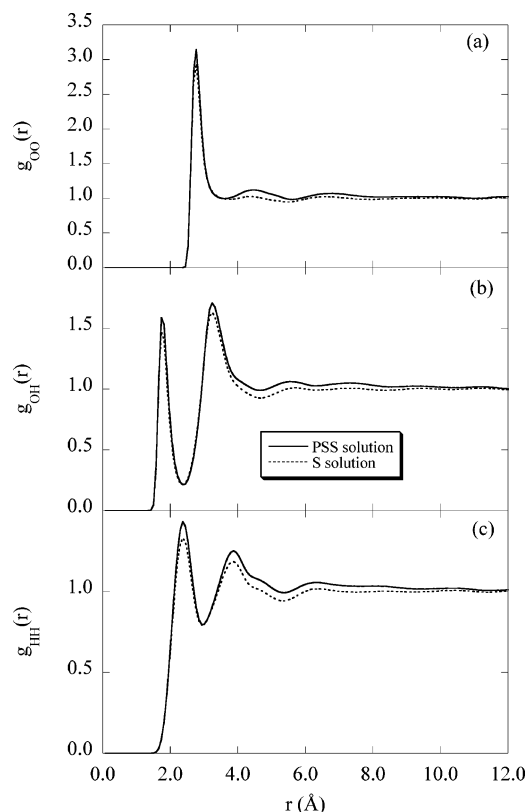
Figure 3. Comparison of the site−site radial distribution functions for water in aqueous polyelectrolyte (PSS) and "backbone-free" (S) solution counterparts with 0.277 m BaCl$_2$ added salt (a) O−O interactions, (b) O−H interactions, (c) H−H interactions.

functions, i.e., $g_{ij}(r \approx 10 \text{ Å}) \approx 1.01-1.03$, indicative of a longer correlation length than that for the aqueous S solution of equivalent ionic strength without chain backbones. In particular, the comparison between the water structure for the PSS and the S aqueous solutions for the same ion molality suggests that the presence of the chain backbone increases the correlation length of the system. Note that an increase of the correlation length is an indication of mechanical destabilization of the system, i.e., incipient phase separation (for a detailed discussion on this phenomenon see Gazzillo[46] and Patey[47]). From a purely microscopic viewpoint, the alluded lengthening of the water correlation length indicates that the solvent's local structural (density) perturbation due to the presence of the chain backbone extends farther away than for smaller/shorter solutes.

The chain perturbation translates into a reduction of the first coordination number, i.e., $n_O^\beta(r_s) = 4\pi\rho_\beta\int_0^{r_s} g_{O\beta}(r)r^2 \, dr$, from $n_O^O(r_s \sim 3.6 \text{ Å}) \approx 6.9$ for the S solutions with 0.277 m added salt to $n_O^O(r_s \sim 3.7 \text{ Å}) \approx 5.3$ to $n_O^O(r_s \sim 3.7 \text{ Å}) \approx 5.3$ for the corresponding S aqueous solutions. Yet, the corresponding first coordination number $n_O^H(r_s)$ stays practically unchanged, i.e., $n_O^H(r_s \sim 2.4 \text{ Å}) \sim 1.7$. Under these circumstances, and assuming a rather loose definition of hydrogen bonding, in that its strength would be given by the value of the $n_O^H(r_s)$, the quoted coordination numbers suggest that the presence of the backbones strengthen the oxygen−oxygen water interactions while preserving the hydrogen bond network. This behavior is consistent with the hydrophobic nature of the uncharged portions of the backbones and the concomitant water density depletion around them.[48,49]

3.2. Water−Counterion Interactions. In Figures 4a−c and 5a−b, we present the radial distributions for the water−ion interactions. According to the structural information for the
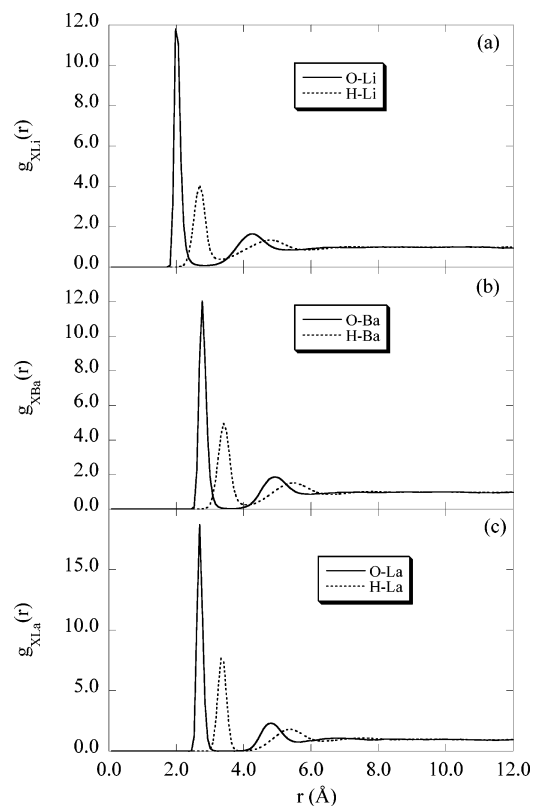

Figure 4. Radial distribution functions for the ion−water interactions in aqueous polyelectrolyte solutions: (a) salt free, (b) 0.277 m BaCl$_2$ added salt, (b) 0.277 m LaCl$_3$ added salt.
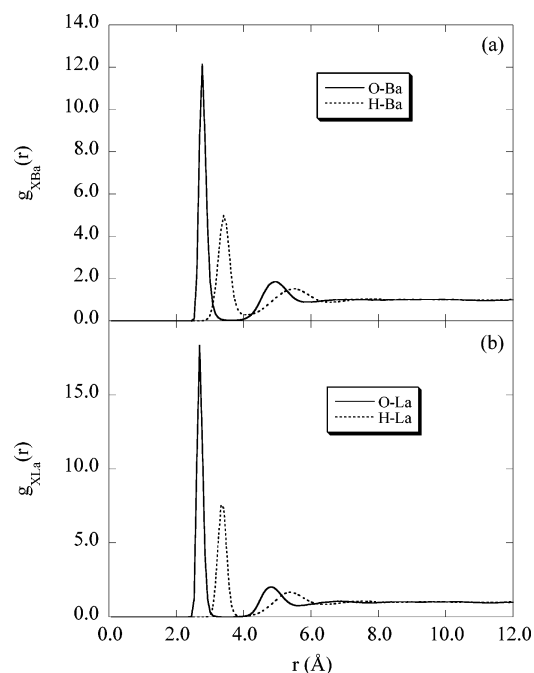

Figure 5. Radial distribution functions for the ion−water interactions in aqueous polyelectrolyte solutions: (a) 0.54 m BaCl$_2$ added salt, (c) 0.54 m LaCl$_3$ added salt.

corresponding S aqueous solutions for the same ionic strength, the solvation behavior of these ions appears to be unaffected by the presence of the backbone chains. In terms of ion coordination numbers, i.e., $n_{M^{z+}}^\beta(r_s) = 4\pi\rho_\beta\int_0^{r_s} g_M^{z+} \beta(r)r^2 \, dr$, Li$^+$ exhibits a first coordination number $n_{Li}^O(r = 3.0 \text{ Å}) \approx 4.0$, while in the case of added salt, Ba^{2+} is coordinated by $n_{Ba}^O(r = 3.2 \text{ Å}) \approx 8.4$ water−oxygens, and La^{3+} by $n_{La}^O(r = 3.5 \text{ Å})$

Polystyrene Sulfonate in Aqueous Electrolyte Solutions

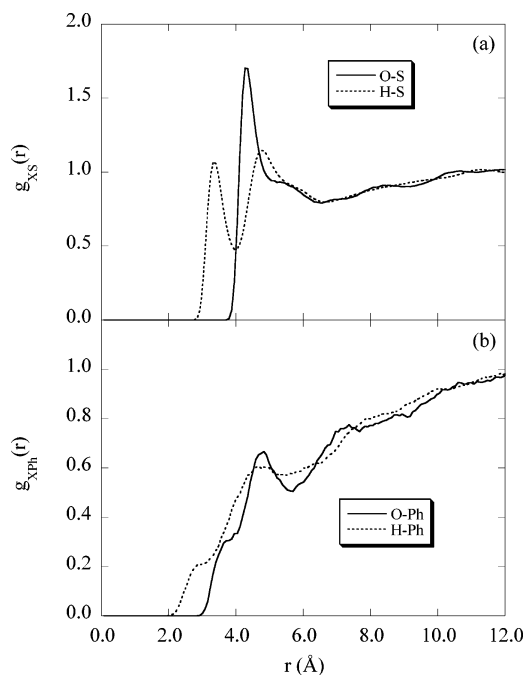*J. Phys. Chem. B, Vol. 109, No. 48, 2005* **23035**

Figure 6. Radial distribution functions for the octamer−water interactions in aqueous polyelectrolyte solutions: (a) phenyl's center of mass−water correlations, (b) sulfonate−water correlations.
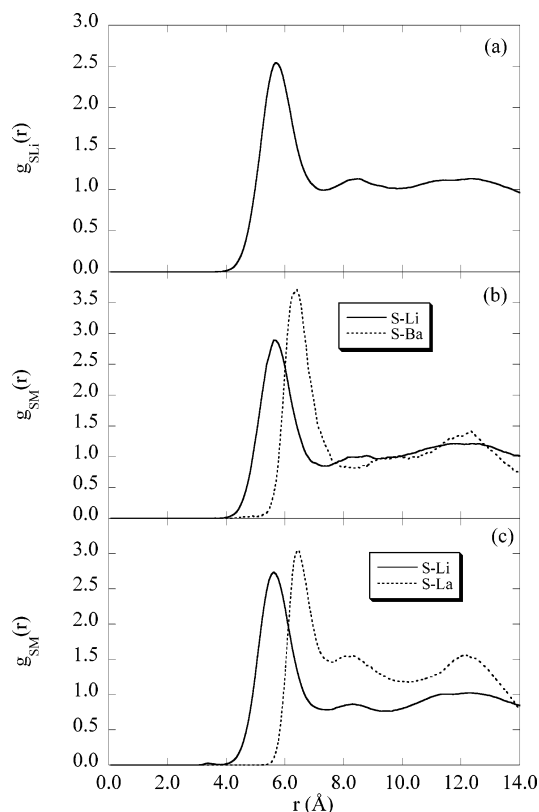

Figure 7. Radial distribution functions for the sulfonate−counterion interactions in aqueous polyelectrolyte solutions: (a) salt-free, (b) 0.277 m BaCl$_2$ added salt, (c) 0.277 m LaCl$_3$ added salt.
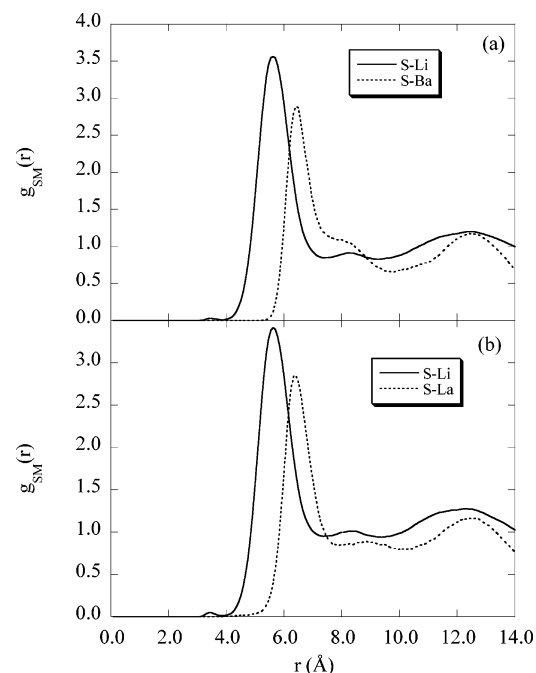

Figure 8. Radial distribution functions for the sulfonate−counterion interactions in aqueous polyelectrolyte solutions: (a) 0.555 m BaCl$_2$ added salt, (b) 0.555 m LaCl$_3$ added salt.

≈ 9.4 water−oxygens. This behavior for the ion coordination is just what we observe for the same cations in S aqueous solutions, i.e., the ions are fully solvated. In fact, the radial distribution functions for the three water−cation interactions show well-defined first water−oxygen coordination peaks, separated by deep valleys from the corresponding second peaks.

3.3. Water−Chain Interactions. In Figure 6a−b, we display the distribution of water around the sulfonated phenyl groups. For that purpose, we determined the radial distribution functions of water around the center of mass of the aromatic rings and the sulfonate groups. The main feature of these radial distribution functions is the clear depletion of the water environment around the center of the phenyl groups and the partial enhancement around the sulfonate groups. This behavior is essentially the same for all systems analyzed here and appears to be independent of the degree of sulfonation and/or distribution of sulfonate groups. In terms of the first coordination numbers $n_S^\beta(r_s) = 4\pi\rho_\beta \int_0^{r_s} g_{S\beta}(r) r^2 \, dr$, the sulfonate groups are surrounded by $n_S^O(r \sim 5 \text{ Å}) \sim 9.6$ water−oxygens, and $n_S^H(r \sim 4 \text{ Å}) \sim 6.7$ water−hydrogens.

3.4. Sulfonate−Counterion Interactions. In Figures 7a−c and 8a−b, we display the radial behavior of the sulfonate−counterion pair distribution functions to assess the strength of the counterion condensation. According to the solvation behavior of the cations (e.g., Figures 4a−c and 5a−b indicate that the first peak of the O−Li$^+$, O−Ba^{2+}, and O−La^{+3} radial distribution functions are located at $\sim$1.95 Å, $\sim$2.77 Å, and $\sim$2.7 Å, respectively), the distributions indicate the formation of solvent-shared ion-pair configurations, i.e., the strength of the sulfonate−cation interactions is not high enough to prevent the cation (or the sulfonate for that matter) from solvating, a behavior not predicted by the primitive model counterparts (see Figure 9).

The presence of polyvalent cations does not affect the location of the first peak of the S$^-$−Li$^+$ radial distribution function (see Figures 7b−c and 8a−b); however, the increase of their concentration appears to strengthen the S$^-$−Li$^+$ correlation. In fact, the comparison between Figures 7b−c and 8a−b clearly indicate the reversal in the relative size of the first peak of the

S$^-$−Li$^+$ and S$^-$−M^{z+} radial distribution function in the presence of Li$^+$, as the polyvalent counterion concentration is doubled. Notably, not only Li$^+$, but also Ba^{2+} and La^{+3} stay solvated when forming the S$^-$−M^{z+} pair, i.e., the three cations form solvent-shared ion pairs with the sulfonate group.

For the definition of the degree of association, according to the procedure of Appendix C, we adopt $d_{-+} \approx 7$ Å for the
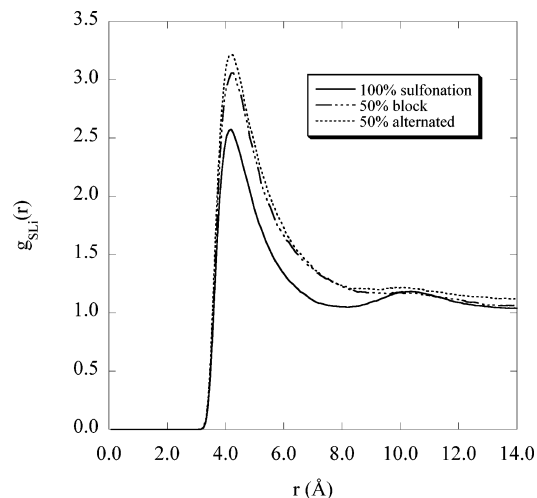
Figure 9. Radial distribution functions for the sulfonate–counterion interactions in salt-free aqueous polyelectrolyte solutions with a primitive solvent with dielectric constant $\epsilon_v = 78$.

TABLE 2: Degree of Association and Conformational Properties of Salt-Free Aqueous Li–PSS Solutions with Explicit Solvent

	100% SO_3^{-a}	50% SO_3^- (block)^b	50% SO_3^- (altern)^c
$\alpha(d_{+-} = 7 \text{ Å})$	0.52 ± 0.01	0.36 ± 0.01	0.34 ± 0.01
R_G (Å)	6.77 ± 0.03	6.01 ± 0.03	6.45 ± 0.03
R_{ee} (Å)	11.4 ± 0.4	9.30 ± 0.15	12.6 ± 0.2

^{a} Fully extended backbone: $R_G \approx 7.28$ Å, $R_{ee} \approx 20.0$ Å. ^{b} Fully extended backbone: $R_G \approx 6.87$ Å, $R_{ee} \approx 20.0$ Å. ^{c} Fully extended backbone: $R_G \approx 6.8$ Å, $R_{ee} \approx 20.0$ Å.

TABLE 3: Degree of Association and Conformational Properties of Salt-Free Aqueous Li–PSS Solutions with a Primitive Solvent with a Dielectric Constant $\epsilon_v = 78$

	100% SO_3^-	50% SO_3^- (block)	50% SO_3^- (altern)
$\alpha(d_{+-} = 7 \text{ Å})$	0.60 ± 0.01	0.45 ± 0.01	0.47 ± 0.01
R_G (Å)	6.99 ± 0.01	6.23 ± 0.01	6.05 ± 0.01
R_{ee} (Å)	8.42 ± 0.01	12.12 ± 0.01	9.43 ± 0.01

S^-–Li^+ and $d_{-+} \approx 8$ Å for the S^-–M^{z+} ion pairs based on the approximate location of the first valley of the radial distribution function for the sulfonate–counterion interactions in aqueous solution (or the location of the inflection point in the corresponding ion-pair distribution function), even for the cases involving a primitive solvent for which the corresponding distribution functions might not show any local minimum after the first peak. According to Tables 2–3, the degree of sulfonation has a strong effect on the counterion condensation in these short oligomers, yet the distribution of sulfonate groups appears to play no role. Similar behavior is predicted by the primitive solvent counterparts.

Note however that the presence of added salt, in particular divalent and trivalent cations, induces an increase in the degree of association (counterion condensation), where Ba^{2+} appears to associate more strongly than La^{+3} for the same concentration of added salt (see Table 4). More precisely, the addition of 0.277 m of $BaCl_2$ appears to be as effective as 0.555 m of $LaCl_3$, and increases the degree of counterion condensation by as much as 25% with respect to the salt-free case. This net increase in the total counterion condensation, when salt is added, is accompanied by a simultaneous decrease in the Li^+ condensation (see Table 4).

TABLE 4: Degree of Association and Effective Charge Li–PSS Solutions with Added Salt and Explicit Solvent

	0.277 m Ba^{2+}	0.277 m La^{3+}	0.555 m Ba^{2+}	0.555 m La^{3+}
$\alpha_+ (d_{-+} = 7 \text{ Å})$	0.46 ± 0.01	0.43 ± 0.01	0.45 ± 0.01	0.43 ± 0.01
$\alpha_{z+} (d_{-+} = 8 \text{ Å})$	0.16 ± 0.01	0.13 ± 0.01	0.21 ± 0.01	0.19 ± 0.01
$(q^{eff}/N_S)(e)$	-0.22 ± 0.01	-0.18 ± 0.01	-0.23 ± 0.01	0.00 ± 0.01

TABLE 5: Degree of Association and Conformational Properties of Aqueous Li–PSS Solutions with Added Salt and Explicit Solvent

	0.277 m Ba^{2+}	0.277 m La^{3+}	0.555 m Ba^{2+}	0.555 m La^{3+}
$\sum_i \alpha_i (d_{-+})^a$	0.63 ± 0.02	0.56 ± 0.02	0.66 ± 0.02	0.62 ± 0.02
R_G (Å)	6.71 ± 0.03	6.84 ± 0.03	6.80 ± 0.03	6.87 ± 0.03
R_{ee} (Å)	9.30 ± 0.1	11.27 ± 0.16	11.27 ± 0.12	13.45 ± 0.16

$^a \sum_i \alpha_i (d_{-+}) = \alpha_+(d_{-+} = 7 \text{ Å}) + \alpha_{z+}(d_{-+} = 8 \text{ Å})$.

Invoking the individual contributions to the degree of association we can define an average effective charge for the PSS backbone in terms of the cancellation of the sulfonate charges by the condensed counterion charges, i.e.,

$$q^{eff} = q^{backbone} + eN_S(\alpha_+ + z\alpha_z^+) \qquad (6)$$

where $q^{backbone} = -eN_S$ is the intrinsic backbone charge, N_S is the number of sulfonate groups in the backbone, e is the electrostatic charge, z is the counterion valence, and α_{z+} is the corresponding degree of counterion condensation.

According to Table 4, the addition of either Ba^{2+} or La^{+3} has a similar effect on the Li^+ condensation, i.e., a 10–20% reduction in its degree of association with respect to the salt-free value (see Table 2). Note that the effective charge in the sulfonate groups is reduced by as much as 80% for all systems with added salt, except for the 0.555 m La^{+3}, for which the charge cancellation is practically complete. The latter behavior is also consistent with the smaller net association exhibited by the 0.555 m La^{+3} solution in contrast to that of the 0.555 m Ba^{+2} case (see Table 5).

3.5. Ion–Counterion Interactions. In the case of aqueous PSS systems with added salts, we have anion–counterion interactions (where anion designates the added anion from the salt; in this case, chloride) in addition to the sulfonate–counterion interactions. This introduces the chance for ion–counterion pair formation from the added salt. For example, according to Figures 10a and 11a, where the added salt is $BaCl_2$, the counterion Li^+ forms a rather strong contact Li^+–Cl^- pair whose peak is located at $r \sim 2.45$ Å, and a less strong solvent-shared pair centered at $r \sim 4.8$ Å. In addition, Ba^{2+} and La^{3+} form a strong contact M^{z+}–Cl^- pair centered at $r \sim 3.1$ Å and as solvent-shared ion pairs centered at $r \sim 5.1$ Å (Figures 10b and 11b), whose strength increases with the concentration of the added salt. Note that the strength of the contact Li^+–Cl^- pair formation in the presence of added salt increases with the doubling of the $BaCl_2$ concentration, though it appears unaffected in the case of $LaCl_3$.

3.6. Sulfonate–Sulfonate Interactions. To check the effect of the degree of dielectric screening (due to the presence of salt) on the S^-–S^- interactions from different chain backbones, i.e., the so-called "like charge attraction", we analyze the behavior of the corresponding radial distribution functions. According to the coordination distances from Figures 3–11, we can infer that the salt-free aqueous PSS solution exhibits a weak solvent-shared S^-–S^- correlation ($r \sim 7.1$ Å) (see Figures 12 and 14a), followed by cation-mediated S^-–S^- pairs ($r \sim$

Polystyrene Sulfonate in Aqueous Electrolyte Solutions

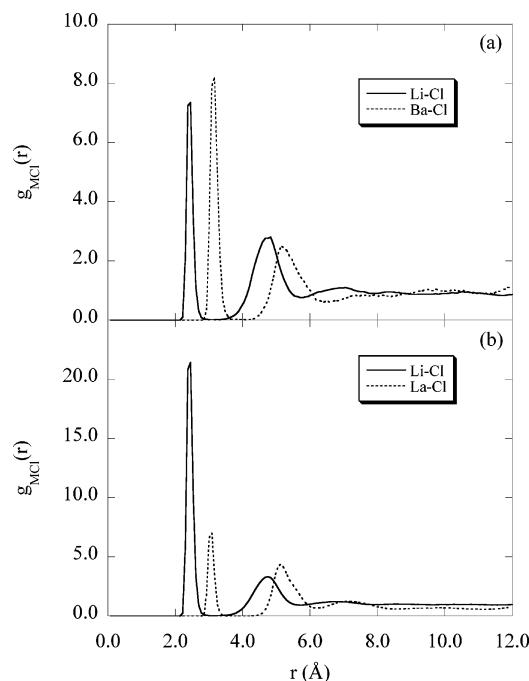*J. Phys. Chem. B, Vol. 109, No. 48, 2005* **23037**

Figure 10. Radial distribution functions for the ion−counterion interactions in aqueous polyelectrolyte solutions: (a) 0.277 m $BaCl_2$ added salt, (b) 0.277 m $LaCl_3$ added salt.
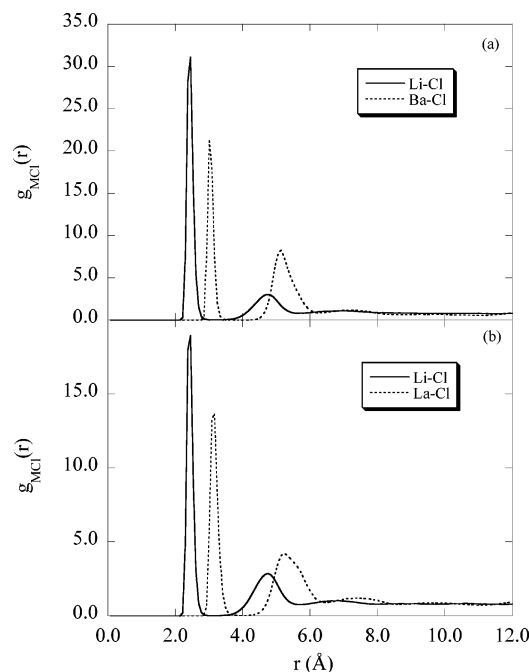

Figure 11. Radial distribution functions for the ion−counterion interactions in aqueous polyelectrolyte solutions: (a) 0.555 m $BaCl_2$ added salt, (b) 0.555 m $LaCl_3$ added salt.

10 Å), i.e., where Li $^+$ as well as Ba^{2+} (La^{3+}) are sandwiched between two sulfonate groups from different backbones forming a configuration as sketched in Figure 14b. The addition of 0.277 m to 0.555 m of either $BaCl_2$ or $LaCl_3$ increases the charge screening and, consequently, increases also the strength of the $S^−$−$S^−$ pair configurations, as clearly depicted in Figure 12. This type of interaction might fall in the category of counterion bridging between two polyelectrolyte chains, known also as *like-charge attraction*, a phenomenon usually detected as electro-viscous effects in simple shear flow of dilute aqueous poly-electrolytes.[50]
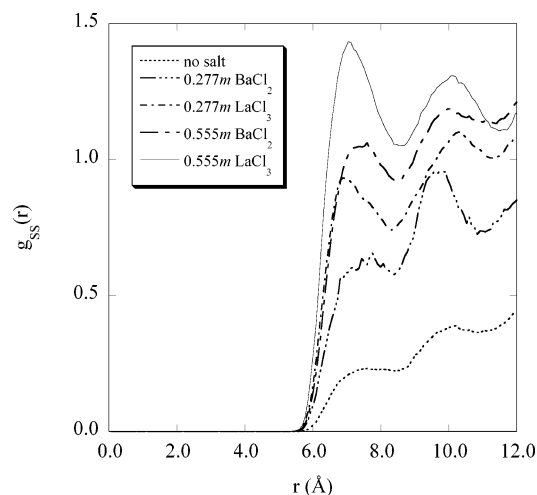

Figure 12. Radial distribution functions for the interchain sulfonate−sulfonate interactions in aqueous polyelectrolyte solutions.
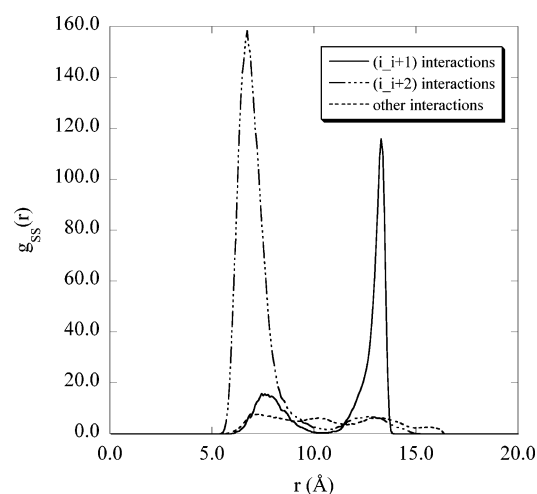

Figure 13. Radial distribution functions for relevant intrachain sulfonate−sulfonate interactions in aqueous polyelectrolyte solutions.

In addition to the alluded interchain $S^−$−$S^−$ interactions, we probed also the intrachain $S^−$−$S^−$ interactions to determine the potentials for *like-charge attraction* mediated by either water or counterions. For that purpose, we determined the radial distribution functions for the seven possible intrachain $S^−$−$S^−$ interactions in the PSS backbones (Figure 13), which clearly indicate two prominent peaks centered at ∼6.75 Å and ∼13.3 Å associated with the intrachain interactions of the ith and (i + 2)th, as well as the ith and (i + 1)th sulfonate groups, respectively. According to the solvation behavior of the sulfonate groups (Figure 6a), the ∼6.75 Å peak in Figures 13 corresponds to a water-mediated intrachain $S^−$−$S^−$ interactions similar to that depicted in Figure 14a for the corresponding interchain $S^−$−$S^−$ interactions, but exhibiting an $S^−OS^−$ ∼ 110°.

3.7. Chain Conformation. According to the results of Table 2, the degree of sulfonation, and the distribution of sulfonate groups in particular, have a clear effect on the backbone conformation of these short chains. Note especially the contrast-ing behavior between the "block" and the "alternated" distribu-tion for the 50% sulfonated chains. This behavior is the result of the mild solvation of the sulfonate groups (Figure 6a) and their complexation with the counterions (Figures 7−8), as opposed to the lack of solvation of the nonsulfonated phenyl groups (Figure 6b). The trend for the conformational properties changes when the explicit atomistic description of the solvent
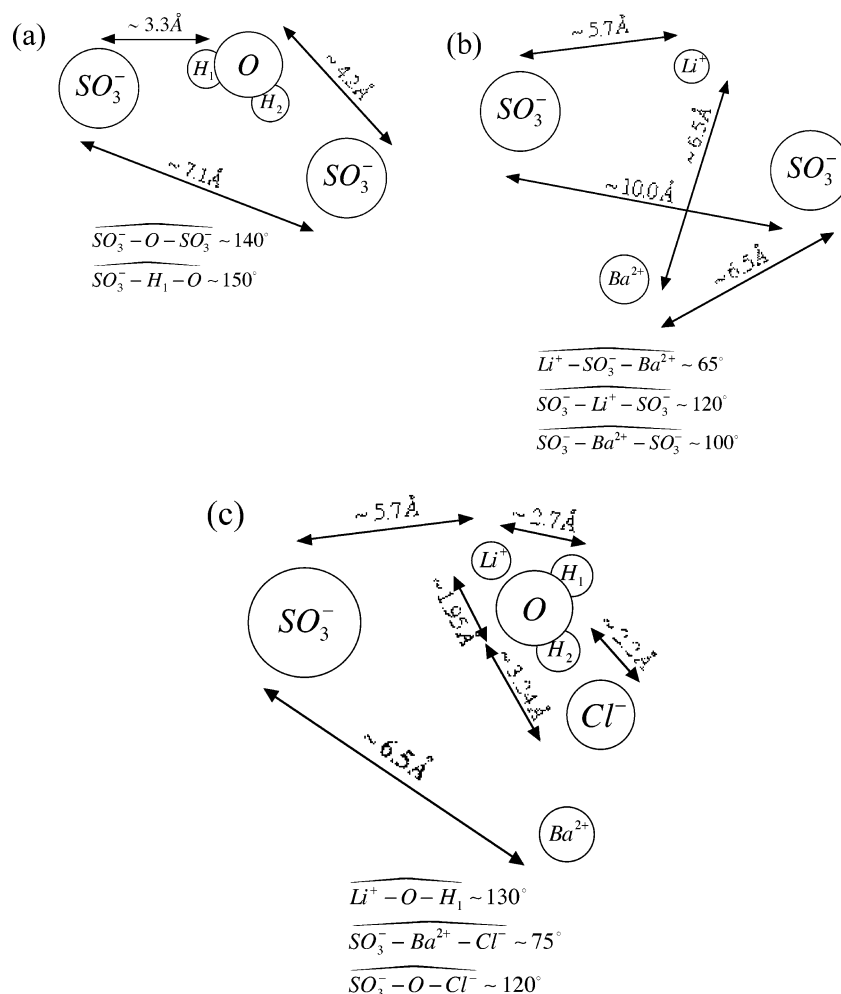
Figure 14. Schematic view of: (a) water-mediated sulfonate−sulfonate attractive interactions, (b) counterion-mediated sulfonate−sulfonate attractive interactions, and (c) counterion−counterion attractive interactions.

is replaced by a primitive continuum dielectric, as indicated in Table 3. Obviously, there is neither solvation nor solvent-shared sulfonate−counterion pair formation (Figure 9), and consequently, the effect of sulfonate distribution on the conformational properties is different from the one observed with explicit solvent.

For the 100% sulfonated backbones, the addition of salt appears to have little or no effect on the root-mean-square radius of gyration of these short chains. In contrast, the corresponding root mean square of the end-to-end distance is either decreased by about 18% with the addition of 0.277 m of BaCl$_2$, or increased by 18% with the addition of 0.555 m of LaCl$_3$. However, the doubling of the BaCl$_2$ or the halving of the LaCl$_3$ concentration shows no effect on the root-mean-square end-to-end distance. This behavior must be related to the peculiar solvation phenomena associated with the sulfonate−counterion interactions and the potential formation of counterion-mediated chain bridges (Figure 14b).

4. Discussion and Final Remarks

The main focus of this work is the solvation behavior of short-chain PSS aqueous solutions in the presence (absence) of added salt. For that purpose, we have placed emphasis on the explicit description of water, the chain backbones, the other species in solution, and the interactions between one another, to analyze specific solvation phenomena determining the structure and conformation of these short-chain PSS aqueous systems. In this

sense, and as far as we are aware, this is one of the first simulation studies involving more than one polyelectrolyte chain and dealing explicitly with atomistic descriptions of all species in solution. In fact, during the preparation of this manuscript, a communication was published by Molnar and Rieger[51] dealing with a fully atomistic simulation of one and two 20-mers Na−PAA chains in aqueous electrolyte solutions, which can be considered the first publication in this regard.

The sets of simulated site−site radial distribution functions that describe the microstructural features of the systems are the "raw data" for an extensive analysis of two relevant solvation phenomena, namely, the counterion condensation in salt-free PSS aqueous solutions, and the ion−coion pair association in PSS aqueous solutions with added salts, whose consequences will be discussed in terms of *like-charge attraction* mechanisms.

A feature frequently found in the conformational behavior of polyelectrolyte aqueous solutions is that the addition of multivalent salt induces a decrease in the magnitude of R_G and R_{ee}, i.e., it makes the chains more compact than those without added salt.[7,52,53] In contrast to the experimentally observed behavior, our simulations indicate that, regardless of the degree of sulfonation and sulfonate distribution, the aqueous octamers exhibit no additional shrinkage (contraction) in the presence of either 0.555 m BaCl$_2$ or 0.555 m LaCl$_3$ over that of the salt-free case. While it might appear that the simulations results are at odds with the experimental evidence, we must recall the wide difference in the backbone lengths, i.e., about 2−3 orders of
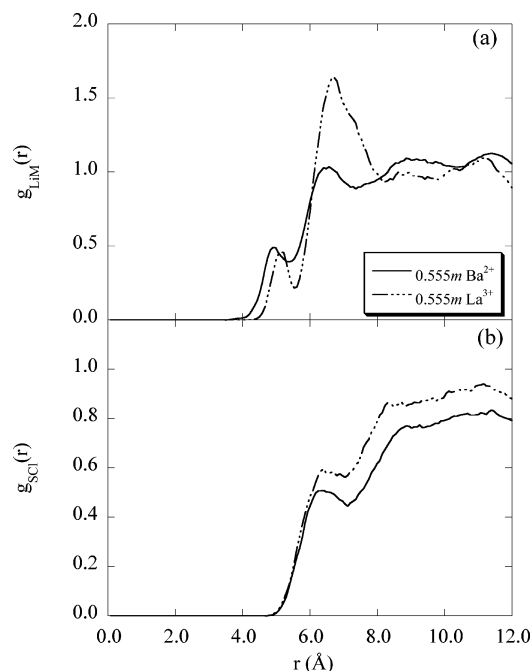
Figure 15. (a) Radial distribution functions for the Li^+-M^{z+} interactions in aqueous polyelectrolyte solutions with the addition of either $BaCl_2$ or $LaCl_3$, (b) radial distribution functions for the S^--Cl^- interactions in aqueous polyelectrolyte solutions with the addition of either $BaCl_2$ or $LaCl_3$.

magnitude (in other words, 8-mers compared with 350- to 5850-mers) and its relevant consequences. In particular, short backbones are relatively more restricted by their intramolecular degrees of freedom (torsional and bending motions) than longer ones, and therefore, their shrinking ability is expected to be correspondingly limited. Our results suggest that the octamer backbones are already approximately shrunk to their minimum length in the presence of the Li^+ counterions, and consequently, the addition of salt with multivalent cations does not contribute to any further backbone shrinkage, at least in terms of the reduction of the root-mean-square radius of gyration R_G. Note that, according to Tables 2 and 5, the decrease of R_G from the initially fully extended backbones to the equilibrium values in all environments is less than 10%.

However, the added salt contributes more significantly to the counterion-mediated bridging between sulfonate groups of neighboring polyelectrolyte chains and concomitant *like-charge attraction*.[50] In fact, we have been able to determine that more subtle *like-charge attraction* (and/or *weaker repulsion*) processes might also occur in the presence of added salt. For example, Figures 14b−c suggest a *like-charge attraction* between the condensed mono- and the polyvalent counterions resulting from the balance of strengths between the $M^{+z}-Cl^-$ pair formation and the S^--M^{z+} condensation. This phenomenon is clearly captured by the Li^+-Ba^{2+} and Li^+-La^{3+} radial distribution functions in Figure 15a. By the same mechanism, we expect persistent S^--Cl^- correlations via a common counterion participating simultaneously in the $M^{+z}-Cl^-$ pair formation and the S^--M^{z+} condensation as depicted in Figure 14c that would result in either a weaker *like-charge repulsion* or even a weak *like-charge attraction*, depending on the ionic strength (Figure 15b). These *like-charge attraction* mechanisms are interdependent and might become the precursors to the formation of chain bundles and subsequent onset of chain precipitation.

While we studied the solvation behavior of the aqueous systems based on realistic nonpolarizable intermolecular po-

tentials models, following the rationale discussed in the Introduction, we are certainly aware of the fact that water is a highly polarizable medium.[54] The polarization effects in these nonpolarizable models are typically accounted for by a set of augmented electrostatic charges that result in a larger water model dipole moment than that for the gas phase (i.e., 1.85 D). The resulting models have been rather successful in describing the behavior of water at normal and extreme conditions, as well as the corresponding aqueous solutions of ions, organics, and gases in either for bulk systems[11,55,56] or interfaces.[57−60]

Despite their success, these models are obviously not able to capture the local inhomogeneities of the polarization of water, such as in the vicinity of charged species and/or interfaces, and the corresponding changes in the dielectric screening of the electrostatic interactions. Several recent studies have involved the explicit use of polarizable models for water and ions[61−64] with the goal of gaining some understanding of the effect of polarization on the solvation behavior of species in solution. However, the main drawback is that the majority of polarizable water models perform rather poorly when used in conditions away from the one used for their parametrization.[65−72] In particular, the disturbing fact that these polarizable models predict the water vapor−liquid envelope in worse agreement than their nonpolarizable counterparts might warrant caution in the interpretation of the simulation results. In this regard, a promising polarizable water model has been recently presented,[73] as a reparametrization of our original version,[74] one that overcomes the pervasive transferability problems found in other models. We are currently working on its application to the study of aqueous electrolyte and polyelectrolyte solutions.

Appendix A: Configurational Temperature for Atomic and Molecular Fluids

On the basis of Rugh's theorem,[75,76] Jepps et al.[77] proposed a more general expression for the calculation of the temperature of classical systems in terms of configurational averages as follows,

$$T = \frac{\langle \nabla H \cdot \boldsymbol{B}(\Gamma) \rangle}{k \langle \nabla \cdot \boldsymbol{B}(\Gamma) \rangle} \tag{A1}$$

where k is the Boltzmann constant, $\boldsymbol{B}(\Gamma)$ is a vector field in terms of the phase-space variable $\Gamma = (\boldsymbol{r}^N, \boldsymbol{p}^N)$ as a function of the spatial coordinates and corresponding conjugate momenta, and $\mathscr{H} \equiv \mathscr{H}(\boldsymbol{r}^N, \boldsymbol{p}^N)$ represents the system Hamiltonian. Jepps et al.[77] as well as Rickaysen and Powles[78] have shown that, depending on the choice of $\boldsymbol{B}(\Gamma)$, it is possible to obtain a series of expressions for the system temperature, including the well-known hypervirial theorems[79] and the energy equipartition theorem. By choosing $\boldsymbol{B}(\Gamma) = \aleph(\Gamma)/(\nabla H(\Gamma) \cdot \aleph(\Gamma))$, where $\aleph(\Gamma)$ is an arbitrary vector field, A1 reduces to a more general form, i.e.,

$$T^{-1} = k \left\langle \nabla H \cdot \left[\frac{\aleph(\Gamma)}{\nabla H \cdot \aleph(\Gamma)} \right] \right\rangle \tag{A2}$$

which makes it possible to determine the system temperature as an average over fully configurational properties. For $\aleph(\Gamma) =$

23040 *J. Phys. Chem. B, Vol. 109, No. 48, 2005*

Chialvo and Simonson

$\nabla U(\boldsymbol{r}^N)$, where $U(\boldsymbol{r}^N)$ is the total intermolecular potential energy, A2 becomes,[77]

$$T^{-1} = k \left| \frac{\nabla^2 U(\boldsymbol{r}^N)}{(\nabla U(\boldsymbol{r}^N))^2} - \frac{2\sum_{ij}^{N} \boldsymbol{f}_i \boldsymbol{f}_j : \nabla_i \boldsymbol{f}_j}{(\sum_i^N f_i^2)^2} \right| \quad \text{(A3)}$$

where obviously $\boldsymbol{f}_i$ is the force on atom i, ∇ is the gradient operator, ∇^2 is the Laplacian operator, and ∇ is the divergence operator.

Typically, for systems involving short-range potentials, the magnitude of the second term of A3 goes as N^{-2}, and therefore, it is usually assumed to be negligibly small. Under this assumption, in the thermodynamic limit, A3 reduces to the following hypervirial expression,[79] i.e.,

$$T = \frac{\langle (\nabla U(\boldsymbol{r}^N))^2 \rangle}{k \langle \nabla^2 U(\boldsymbol{r}^N) \rangle} \quad \text{(A4)}$$

Moreover, for atomic systems under pairwise additivity, A4 becomes,

$$T = -\langle \sum_{i=1}^{N} f_i^2 \rangle / k \langle \sum_{i=1}^{N} \nabla \cdot \boldsymbol{f}_i \rangle \quad \text{(A5)}$$

while for molecular systems, whose molecular integrity is kept through the use of constraints, A4 becomes,[42]

$$T = -\langle \sum_{i=1}^{N} \sum_{\alpha=1}^{n} f_{i\alpha}^2 \rangle / k \langle \sum_{i=1}^{N} \sum_{\alpha=1}^{n} \nabla_\alpha \cdot \boldsymbol{f}_{i\alpha} \rangle \quad \text{(A6)}$$

where α denotes a site on molecule i, and N is the total number of molecular species. Otherwise, for rigid molecules, a hypervirial orientational analogous to A4 can be used,[80] i.e.,

$$T = \frac{\langle (\nabla_\theta U(\boldsymbol{r}^N, \omega^N))^2 \rangle}{k \langle \nabla_\theta^2 U(\boldsymbol{r}^N, \omega^N) \rangle} \quad \text{(A7)}$$

where ∇_θ and ∇_θ^2 are the angular gradient and Laplacian operators, respectively.

For the system under study, we have a mixture of rigid and flexible molecules plus spherical ions, therefore, the configurational temperature of the mixture becomes,

$$T = -k^{-1} \left| \frac{\sum_{i=1}^{\text{chains}} \sum_{\alpha=1}^{\text{sites}} f_{i\alpha}^2 + \sum_{i=1}^{\text{waters}} \sum_{\alpha=1}^{3} f_{i\alpha}^2 + \sum_{i=1}^{\text{ions}} f_i^2}{\sum_{i=1}^{\text{chains}} \sum_{\alpha=1}^{\text{sites}} \nabla_\alpha \cdot \boldsymbol{f}_{i\alpha} + \sum_{i=1}^{\text{waters}} \sum_{\alpha=1}^{3} \nabla_\alpha \cdot \boldsymbol{f}_{i\alpha} + \sum_{i=1}^{\text{ions}} \nabla_\alpha \cdot \boldsymbol{f}_i} \right| \quad \text{(A8)}$$

We also analyze portions of the system, such as those comprising only the water molecules, the ions, or the backbones, so that,

$$T = -k^{-1} \left| \frac{\sum_{i=1}^{\text{chains}} \sum_{\alpha=1}^{\text{sites}} f_{i\alpha}^2}{\sum_{i=1}^{\text{chains}} \sum_{\alpha=1}^{\text{sites}} \nabla_\alpha \cdot \boldsymbol{f}_{i\alpha}} \right| = -k^{-1} \left| \frac{\sum_{i=1}^{\text{waters}} \sum_{\alpha=1}^{3} f_{i\alpha}^2}{\sum_{i=1}^{\text{waters}} \sum_{\alpha=1}^{3} \nabla_\alpha \cdot \boldsymbol{f}_{i\alpha}} \right| = \\ -k^{-1} \left| \frac{\sum_{i=1}^{\text{ions}} f_i^2}{\sum_{i=1}^{\text{ions}} \nabla_\alpha \cdot \boldsymbol{f}_i} \right| \quad \text{(A9)}$$

Note that we should expect a small deviation from the thermodynamic limit of the calculated configurational temperature according to either A8 or A9 due to our neglecting of the second term in A3 for systems involving long-range electrostatic interactions.[77]

Appendix B: Interaction Potentials Parameters for the Aqueous Electrolyte Polystyrene Sulfonate Solutions

TABLE B1: Lennard−Jones Potential Parameters and Coulombic Charges

group/species	σ_{ii} (Å)	ϵ_{ii}/k (K)	q_i (e)
$n-CH_2$, $-CH_3$	3.850	60.43	0
$-CH$	3.700	45.32	0
$-C^{arom}$, $-CH^{arom}$	3.700	60.43	0
$-SO_3^-$	6.00	251.80	-1
$-O_{SPC/E}$	3.166	78.23	-0.8476
Li^+	2.023	9.21	1
Ba^{2+}	3.784	23.7	2
La^{3+}	3.75	30.21	3

TABLE B2: Bending Potential Parameters

bending angle	k_θ^{chain} (kJ/mol)	θ_o^{chain} (deg)
$-CH_2-CH-CH_2$	251.16	109.5
$-CH_2-CH^{aliph}-CH^{arom}$	251.16	109.5
$CH^{aliph}-CH_2-CH^{aliph}$	263.72	109.5
$-CH^{aliph}-CH^{arom}-CH^{arom}$	293.02	120.0
$-CH^{arom}-CH^{arom}-CH^{arom}$	301.0	120.0
$-CH^{arom} - CH^{arom} - SO_3^-$	301.0	120.0

TABLE B3: Torsional Potential Parameters

k_χ (kJ/mol)	8.37
χ_o (degrees)	90.0
k_ψ (kJ/mol)	334.9
k_φ^{arom} (kJ/mol)	54.0
k_φ^{aliph} (kJ/mol)	5.86
θ_o^{imp} (deg)	109.5

TABLE B4: Bond-Length Distances

group−group	l_{ij} (Å)
$-CH_2-CH$	1.53
$-CH^{alip} -CH^{arom}$	1.51
$-CH^{arom}-CH^{arom}$	1.40
$-CH^{arom}-SO_3^-$	1.53

Appendix C: Definition of Degree of $SO_3^- - M^{z+}$ Pair Association and its Relation to the Radial Distribution Function $g_{SO_3^- - M^{z+}}(r)$

Given the fact that most radial pair distribution functions are available by simulation, in particular, the ones for the sulfonate−cation interactions, it is rather convenient to be able to use this structural information to assess the degree of sulfonate−cation association. While this approach is theoretically straightforward for the limiting case of infinite dilution,[40] it becomes more

Polystyrene Sulfonate in Aqueous Electrolyte Solutions

J. Phys. Chem. B, Vol. 109, No. 48, 2005 **23041**

cumbersome and less obvious at finite salt concentrations. For that purpose, here we apply a rigorous, yet little known theoretical approach developed more than forty years ago by Poirier and DeLap,[45] and then we devise a simulation scheme to assess the degree of association for all cases, in particular, for those cases, e.g., multicounterions, where the above formalism cannot provide explicit expressions for the degree of association in terms of the corresponding $g_{SO_3^- - M^{z+}}(r)$. For the case considered here, i.e., $z = 1$, the degree of $SO_3^- - M^+$ pair association, α_{-+}, is defined as,

$$\alpha_{-+} = \int_0^{d_{-+}} G_{-+}(r) dr \qquad (C1)$$

where d_{-+} denotes the largest distance where the $SO_3^- - M^+$ pairs are counted, typically the location of the first valley of $g_{SO_3^- - M^+}(r)$, and $G_{-+}(r)\Delta r$ is the probability of finding the SO_3^- group in the spherical shell of thickness Δr, separated by a distance r from the M^+ ion, when neither the SO_3^- nor the M^+ forms any additional pair within r. From a statistical mechanical point of view, $G_{-+}(r)$ can be written as the following integral equation,

$$G_{-+}(r) = 4\pi\rho_+ g_{-+}(r) r^2 P_-(r) P_+(r) \qquad (C2)$$

where $P_-(r)$ ($P_+(r)$) denotes the probability that an SO_3^-(M^+) separated by a distance r from an M^+(SO_3^-) does not form an ion pair with any other ion of the opposite charge, i.e.,

$$P_-(r) = 1 - \int_0^r G_{-+}(s) ds$$

$$P_+(r) = 1 - \int_0^r G_{+-}(s) ds \qquad (C3)$$

Therefore, the entire formalism hinges around being able to determine $P_-(r)$ and $P_+(r)$ through the simultaneous solution of C2−C3, under the following obvious boundary condition,

$$\rho_- G_{-+}(r) = \rho_+ G_{+-}(r) \qquad (C4)$$

since $g_{-+}(r) = g_{+-}(r)$. For the present case, by considering C3−C4, we obviously have $P_-(r) = P_+(r)$ and $\rho_+ = \rho_-$, and by solving the integral equation, it follows that,

$$P_-(r) = [1 + 4\pi\rho_+ \int_0^r g_{-+}(s)s^2 ds]^{-1} \qquad (C5)$$

Finally, from C2−C5,

$$G_{-+}(r) = 4\pi\rho_+ g_{-+}(r) r^2/[1 + 4\pi\rho_+ \int_0^r g_{-+}(s)s^2 ds]^2 \quad (C6)$$

which satisfies the required normalization, i.e.,

$$\int_0^\infty G_{-+}(r) dr = 1 - [1 + 4\pi\rho_+ \int_0^\infty g_{-+}(r)s^2 dr]^{-1} = 1 \qquad (C7)$$

According to the Poirier and DeLap formalism, similar expressions can be derived for asymmetric ion pairs, as discussed in the original paper.

Of course, it is also possible to determine the ion-pair radial distribution function $G_{-+}(r)$ directly by the corresponding histogram. While this might not be necessary, as long as we have an explicit expression for the degree of association in terms of the $g_{-+}(r)$, it becomes crucial for those cases where the formalism does not provide it, such as PSS aqueous solutions with added salts.
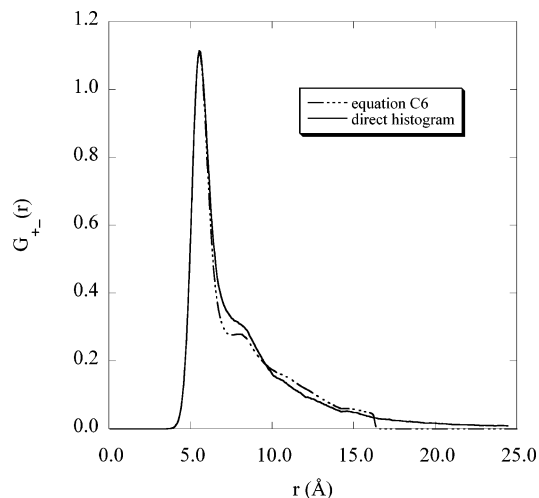

Figure 16. Comparison between the profile of $G_{-+}(r)$ given by eq C6, using the $g_{-+}(r)$ from simulation (note the truncation around $r \sim$ 16 Å), and that from the direct determination of the histogram as described in Appendix C.

For each system configuration, we know the relative location of each $SO_3^- - M^+$ pair so that, out of the entire set of distances, we choose the closest one. After recording this distance and the corresponding particle indices, we remove the closest ion pair from further consideration and choose the next closest ion pair from the remaining $2N_{SO_3^-} - 2SO_3^- - M^+$ pairs. Thus, we continue this process until each SO_3^- is paired to one M^+, and in doing so for each configuration, we obtain the cumulative histogram from which we can assess the corresponding average distribution (eq C2). Note that, for the cases for which Poirier and DeLap formalism provides the explicit expression such as C6, the suggested alternative scheme provides an additional test of internal consistency. An example for such a test is given in Figure 16, where we compare the behavior of $G_{-+}(r)$ determined by C6 via the simulated $g_{-+}(r)$, and the corresponding profile obtained by the direct histogram.

References and Notes

(1) Delsanti, M.; Dalbiez, J. P.; Spalla, O.; Belloni, L.; Drifford, M. Phase Diagram of Polyelectrolyte Solutions in the Presence of Multivalent Salts. In *Macro-Ion Characterization. From Dilute Solutions to Complex Fluids*; Schmitz, K. S., Ed.; American Chemical Society: Washington, D. C., 1994; Vol. 548; p 381.

(2) Angelini, T. E.; Liang, H.; Wriggers, W.; Wong, G. C. L. *Proc. Natl. Acad. Sci. U.S.A.* **2003**, *100*, 8634.

(3) Grosberg, A. Y.; Nguyen, T. T.; Shklovskii, B. I. *Rev. Mod. Phys.* **2002**, *74*, 329.

(4) Silva, M. B. A.; Kuhn, P. S.; Lucena, L. S. *Physica A* **2001**, *296*, 31.

(5) Koculi, E.; Lee, N. K.; Thirumalai, D.; Woodson, S. A. *J. Mol. Biol.* **2004**, *341*, 27.

(6) Hinderberger, D.; Jeschke, G.; Spiess, H. W. *Colloid Polym. Sci.* **2004**, *282*, 901.

(7) Zhang, Y. B.; Douglas, J. F.; Ermi, B. D.; Amis, E. J. *J. Chem. Phys.* **2001**, *114*, 3299.

(8) Olvera de la Cruz, M.; Belloni, L.; Delsanti, M.; Dalbiez, J. P.; Spalla, O.; Drifford, M. *J. Chem. Phys.* **1995**, *103*, 5781.

(9) Essafi, W.; Lafuma, F.; Williams, C. E. *J. Phys. II* **1995**, *5*, 1269.

(10) Huang, C. I.; de la Cruz, M. O. *Macromolecules* **2002**, *35*, 976.

(11) Chialvo, A. A.; Cummings, P. T. Molecular-Based Modeling of Water and Aqueous Solutions at Supercritical Conditions. In *Advances in Chemical Physics*; Rice, S. A., Ed.; Wiley & Sons: New York, 1999; Vol. 109; p 105.

(12) Sinn, C. G.; Dimova, R.; Antonietti, M. *Macromolecules* **2004**, *37*, 3444.

(13) Carbaja-Tinoco, M. D.; Ober, R.; Dolbnya, I.; Bras, W.; Williams, C. E. *J. Phys. Chem. B* **2002**, *106*, 12165.

(14) Roberts, J. M.; O'Dea, J. J.; Osteryoung, J. G. *Anal. Chem.* **1998**, *70*, 3667.

(15) Qu, D.; Baigl, D.; Williams, C. E.; Mohwald, H.; Fery, A. *Macromolecules* **2003**, *36*, 6878.

(16) Bohme, U.; Scheler, U. *Colloids Surf., A* **2003**, *222*, 35.

(17) Bordi, F.; Cametti, C.; Tan, J. S.; Boris, D. C.; Krause, W. E.; Plucktaveesak, N.; Colby, R. H. *Macromolecules* **2002**, *35*, 7031.

(18) Bordi, F.; Cametti, C.; Gili, T. *Phys. Rev. E* **2003**, *68*.

(19) Volk, N.; Vollmer, D.; Schmidt, M.; Oppermann, W.; Huber, K. Conformation and Phase Diagrams of Flexible Polyelectrolytes. In *Polyelectrolytes with Defined Molecular Architecture II*; Springer: Berlin, 2004; Vol. 166; p 29.

(20) Lindsay, H. M.; Chaikin, P. M. *J. Chem. Phys.* **1982**, *76*, 3774.

(21) Larsen, A. E.; Grier, D. G. *Nature* **1997**, *385*, 230.

(22) Romet-Lemonne, G.; Daillant, J.; Guenoun, P.; Yang, J.; Holley, D. W.; Mays, J. W. *J. Chem. Phys.* **2005**, *122*.

(23) Muller, F.; Guenoun, P.; Delsanti, M.; Deme, B.; Auvray, L.; Yang, J.; Mays, J. W. *Eur. Phys. J. E* **2004**, *15*, 465.

(24) Chang, R. W.; Yethiraj, A. *J. Chem. Phys.* **2003**, *118*, 11315.

(25) Micka, U.; Holm, C.; Kremer, K. *Langmuir* **1999**, *15*, 4033.

(26) Aqvist, J. *Journal of Physical Chemistry* **1990**, *94*, 8021.

(27) van Veggel, F.; Reinhoudt, D. N. *Chem.—Eur. J.* **1999**, *5*, 90.

(28) Winkler, R. G.; Gold, M.; Reineker, P. *Phys. Rev. Lett.* **1998**, *80*, 3731.

(29) Liu, S.; Ghosh, K.; Muthukumar, M. *J. Chem. Phys.* **2003**, *119*, 1813.

(30) Berendsen, H. J. C.; Grigera, J. R.; Straatsma, T. P. *J. Phys. Chem.* **1987**, *91*, 6269.

(31) Smith, D. E.; Dang, L. X. *J. Chem. Phys.* **1994**, *100*, 3557.

(32) Lyulin, A. V.; Michels, M. A. J. *Macromolecules* **2002**, *35*, 1463.

(33) Mondello, M.; Yang, H. J.; Furuya, H.; Roe, R. J. *Macromolecules* **1994**, *27*, 3566.

(34) Faeder, J.; Ladanyi, B. M. *J. Phys. Chem. B* **2000**, *104*, 1033.

(35) Martyna, G. J.; Tuckerman, M. E.; Tobias, D. J.; Klein, M. L. *Mol. Phys.* **1996**, *87*, 1117.

(36) Cheng, A. L.; Merz, K. M. *J. Phys. Chem.* **1996**, *100*, 1927.

(37) Ryckaert, J. P.; Ciccotti, G.; Berendsen, H. J. C. *J. Comput. Phys.* **1977**, *23*, 327.

(38) Andersen, H. C. *J. Comput. Physics* **1983**, *52*, 24.

(39) Palmer, B. J. *J. Comput. Phys.* **1993**, *104*, 470.

(40) Chialvo, A. A.; Cummings, P. T.; Cochran, H. D.; Simonson, J. M.; Mesmer, R. E. *J. Chem. Phys.* **1995**, *103*, 9379.

(41) Chialvo, A. A.; Cummings, P. T.; Simonson, J. M.; Mesmer, R. E. *J. Chem. Phys.* **1996**, *105*, 9248.

(42) Lue, L.; Evans, D. J. *Phys. Rev. E* **2000**, *62*, 4764.

(43) Destree, M.; Laupretre, F.; Lyulin, A.; Ryckaert, J. P. *J. Chem. Phys.* **2000**, *112*, 9632.

(44) Fincham, D. *Mol. Simul.* **1994**, *13*, 1.

(45) Poirier, J. C.; DeLap, J. H. *J. Chem. Phys.* **1961**, *35*, 213.

(46) Gazzillo, D. *Mol. Phys.* **1994**, *83*, 1171.

(47) Ursenbach, C. P.; Patey, G. N. *J. Chem. Phys.* **1994**, *100*, 3827.

(48) Czaplewski, C.; Liwo, A.; Ripoll, D. R.; Scheraga, H. A. *J. Phys. Chem. B* **2005**, *109*, 8108.

(49) Zou, Q.; Bennion, B. J.; Daggett, V.; Murphy, K. P. *J. Am. Chem. Soc.* **2002**, *124*, 1192.

(50) Pu, Q.; Ng, S.; Mok, V.; Chen, S. B. *J. Phys. Chem. B* **2004**, *108*, 14124.

(51) Molnar, F.; Rieger, J. *Langmuir* **2005**, *21*, 786.

(52) Dubois, E.; Boue, F. *Macromolecules* **2001**, *34*, 3684.

(53) Schweins, R.; Lindner, P.; Huber, K. *Macromolecules* **2003**, *36*, 9564.

(54) Chialvo, A. A.; Cummings, P. T. *J. Chem. Phys.* **1996**, *105*, 8274.

(55) Guillot, B.; Guissani, Y. *Mol. Phys.* **1993**, *79*, 53.

(56) Kalinichev, A. G. *Rev. Mineral. Geochem.* **2001**, *42*, 83.

(57) Benjamin, I. *Annu. Rev. Phys. Chem.* **1997**, *48*, 407.

(58) Predota, M.; Bandura, A. V.; Cummings, P. T.; Kubicki, J. D.; Wesolowski, D. J.; Chialvo, A. A.; Machesky, M. L. *J. Phys. Chem. B* **2004** *108*, 12049.

(59) Striolo, A.; Gubbins, K. E.; Chialvo, A. A.; Cummings, P. T. *Mol. Phys.* **2004**, *102*, 243.

(60) Vacha, R.; Slavicek, P.; Mucha, M.; Finlayson-Pitts, B. J.; Jungwirth, P. *J. Phys. Chem. A* **2004**, *108*, 11573.

(61) Kim, B. C.; Young, T.; Harder, E.; Friesner, R. A.; Berne, B. J. *J. Phys. Chem. B* **2005**, *109*, 16529.

(62) Mucha, M.; Frigato, T.; Levering, L. M.; Allen, H. C.; Tobias, D. J.; Dang, L. X.; Jungwirth, P. *J. Phys. Chem. B* **2005**, *109*, 7617.

(63) Dang, L. X.; Schenter, G. K.; Fulton, J. L. *J. Phys. Chem. B* **2003**, *107*, 14119.

(64) Tuma, L.; Jenicek, D.; Jungwirth, P. *Chem. Phys. Lett.* **2005**, *411*, 70.

(65) Dang, L. X.; Chang, T. M.; Panagiotopoulos, A. Z. *J. Chem. Phys.* **2002**, *117*, 3522.

(66) Yezdimer, E.; Cummings, P. T. *Mol. Phys.* **1999**, *97*, 993.

(67) Hayward, T. M.; Svishchev, I. M. *Fluid Phase Equilib.* **2001**, *182*, 65.

(68) Yoshii, N.; Miyauchi, R.; Miura, S.; Okazaki, S. *Chem. Phys. Lett.* **2000**, *317*, 414.

(69) Yoshii, N.; Yoshie, H.; Miura, S.; Okazaki, S. *Rev. High Pressure Sci. Technol.* **1998**, *7*, 1115.

(70) Kiyohara, K.; Gubbins, K. E.; Panagiotopoulos, A. Z. *Mol.r Phys.* **1998**, *94*, 803.

(71) Rivera, J. L.; Predota, M.; Chialvo, A. A.; Cummings, P. T. *Chem. Phys. Lett.* **2002**, *357*, 189.

(72) Jedlovszky, P.; Vallauri, R. *J. Chem. Phys.* **2005**, *122*.

(73) Paricaud, P.; Predota, M.; Chialvo, A. A.; Cummings, P. T. *J. Chem. Phys.* **2005**, *122*.

(74) Chialvo, A. A.; Cummings, P. T. *Fluid Phase Equilib.* **1998**, *150*–*151*, 73.

(75) Rugh, H. H. *Phys. Rev. Lett.* **1997**, *78*, 772.

(76) Rugh, H. H. *J. Phys. A: Math. Gen.* **1998**, *31*, 7761.

(77) Jepps, O. G.; Ayton, G.; Evans, D. J. *Phys. Rev. E* **2000**, *62*, 4757.

(78) Rickayzen, G.; Powles, J. G. *J. Chem. Phys.* **2001**, *114*, 4333.

(79) Hirschfelder, J. O. *J. Chem. Phys.* **1960**, *33*, 1462.

(80) Chialvo, A. A.; Simonson, J. M.; Kusalik, P. G.; Cummings, P. T. *AICHE Symp. Ser.* **2001**, *97*, 273.